The novel intestinal filament organizer IFO-1 contributes to epithelial integrity in concert with ERM-1 and DLG-1

Katrin Carberry[1],*, Tobias Wiesenfahrt[1],*, Florian Geisler[1], Stephanie Stöcker[1], Harald Gerhardus[1], Daniel Überbach[1], Wayne Davis[2], Erik Jorgensen[2], Rudolf E. Leube[1],‡ and Olaf Bossinger[1],‡

SUMMARY

The nematode *Caenorhabditis elegans* is an excellent model system in which to study in vivo organization and function of the intermediate filament (IF) system for epithelial development and function. Using a transgenic *ifb-2::cfp* reporter strain, a mutagenesis screen was performed to identify mutants with aberrant expression patterns of the IF protein IFB-2, which is expressed in a dense network at the subapical endotube just below the microvillar brush border of intestinal cells. Two of the isolated alleles (*kc2* and *kc3*) were mapped to the same gene, which we refer to as *ifo-1* (intestinal filament organizer). The encoded polypeptide colocalizes with IF proteins and F-actin in the intestine. The apical localization of IFO-1 does not rely on IFB-2 but is dependent on LET-413, a basolateral protein involved in apical junction assembly and maintenance of cell polarity. In mutant worms, IFB-2 and IFC-2 are mislocalized in cytoplasmic granules and accumulate in large aggregates at the *C. elegans* apical junction (CeAJ) in a DLG-1-dependent fashion. Electron microscopy reveals loss of the prominent endotube and disordered but still intact microvilli. Semiquantitative fluorescence microscopy revealed a significant decrease of F-actin, suggesting a general role of IFO-1 in cytoskeletal organization. Furthermore, downregulation of the cytoskeletal organizer ERM-1 and the adherens junction component DLG-1, each of which leads to F-actin reduction on its own, induces a novel synthetic phenotype in *ifo-1* mutants resulting in disruption of the lumen. We conclude that IFO-1 is a multipurpose linker between different cytoskeletal components of the *C. elegans* intestinal terminal web and contributes to proper epithelial tube formation.

KEY WORDS: *Caenorhabditis elegans*, Epithelial cell polarity, Intestine, Intermediate filaments, F-actin

INTRODUCTION

Intermediate filaments (IFs), actin filaments (AFs) and microtubules are the main components of the cytoskeleton. Besides their different structural and functional properties they form an interactive and integrated network that is involved in all major cellular functions and processes, such as the transport of vesicles or organelles, the regulation of cell division and cell motility and the establishment of cell polarity. In order to perform these tasks, the different filament types have to be restructured and modulated in a coordinated fashion (Fletcher and Mullins, 2010). IFs form resilient but flexible filaments and their main purpose is to protect cells against mechanical stress, though other functions in regulation of cell growth, cell death and response to non-mechanical stresses have been described (Kim and Coulombe, 2007; Toivola et al., 2010). Depending on the cell type and cell cycle stage IFs are very differently arranged. They form intricate three dimensional networks in cultured cells, thick bundles in keratinocytes and neurons, granules in mitotic cells or dense fibrous sheets below the apical terminal web of intestinal cells (Iwatsuki and Suda, 2010). How these different types of spatial arrangement are established and maintained is not very well understood.

C. elegans provides an excellent system for studying the dynamics and regulation of IF networks. Its genome contains 11 cytoplasmic IF genes, six of which are predominantly expressed in the intestine (Carberry et al., 2009). The *C. elegans* intestine consists of only 20 cells, which form a single layered, simple epithelial tube (Leung et al., 1999; Sulston et al., 1983). The IFs form a thick perilumenal network that is localized below the microvillar brush border and is anchored to the CeAJ (Bossinger et al., 2004; Hüsken et al., 2008; Karabinos et al., 2002; Karabinos et al., 2004). On top rest the microvillar rootlets that are connected to each other via the terminal web, which consists of a mesh of various cytoskeletal filaments (Hirokawa et al., 1982; Kormish et al., 2010; McGhee, 2007). The *C. elegans* intestine is particularly rich in IFs and is characterized by the nematode-specific electron-dense and IF-containing endotube (Bossinger et al., 2004; Munn and Greenwood, 1984). To identify and examine molecular regulators that are responsible for the highly specific subcellular enrichment of the intestinal IFs in *C. elegans*, a mutagenesis screen was performed using an IFB-2::CFP reporter that is expressed exclusively in the intestinal endotube (Hüsken et al., 2008). The highly specific and strong IFB-2::CFP fluorescence is ideally suited for large-scale screening using epifluorescence. Here, we identify and perform in-depth analysis of two alleles, *kc2* and *kc3*, of ORF F42C5.10 encoding the novel intestinal filament organizer IFO-1.

MATERIALS AND METHODS

DNA constructs

Constructs encoding IFO-1::YFP and IFO-1::CFP were prepared by amplifying the 1256 bp *ifo-1* promoter from genomic DNA (amplimers: 5′-CCGCCGAAGCTTTGGTTTTAAATTGTATTTTATAG-3′, 5′-CCGC-CGAAGCTTGCTGAAATCGTATTCGAATTTTG-3′) and inserting the *Hin*dIII-cleaved fragment into the *yfp*- and *cfp*-containing vectors pVH20.01 and pVH10.10 (Hutter, 2003) generating pP*ifo-1::yfp* and pP*ifo-*

[1]Institute of Molecular and Cellular Anatomy (MOCA), RWTH Aachen University, D-52074 Aachen, Germany. [2]Department of Biology and Howard Hughes Medical Institute, University of Utah, Salt Lake City, UT 84112-0840, USA.

*These authors equally contributed to this work
‡Authors for correspondence (rleube@ukaachen.de; olaf.bossinger@rwth-aachen.de)

1::cfp, respectively. For cloning of the 3897 bp *ifo-1* cDNA fragment, total RNA was prepared (RNeasy Minikit, Qiagen) and reverse transcribed (Omniscript RT kit, Qiagen). *ifo-1* cDNA was then amplified by PCR (primers: 5′-ATCATCGGATCCATGGGAGACCTACAAGTCGAC-3′, 5′-TCCTCCGGATCCAAATTTGGTCCATCGCCGG-3′). The *Bam*HI-digested product was inserted into pP*ifo-1::yfp* and pP*ifo-1::cfp*.

C. elegans strains and culture

Standard *C. elegans* handling procedures have been described (Brenner, 1974). Hawaiian strain CB4856 was used for single nucleotide polymorphism (SNP)-mapping and Bristol strain N2 was used as wild type (WT) (both from *Caenorhabditis* Genetics Center, University of Minnesota). VJ311 [*erm-1(tm677)*] was provided by S. Mitani (Tokyo Women's Medical University School of Medicine, Japan). BJ52 *kcIs21[ifb2::cfp]V* (Hüsken et al., 2008) was used for mutagenesis. *ifo-1* mutants carrying allele *kc2* were BJ133 *kcIs21[ifb-2::cfp]V;ifo-1(kc2)IV* and BJ142 *ifo-1(kc2)IV*. *ifo-1* mutants carrying allele *kc3* were BJ134 *kcIs21[ifb-2::cfp]V;ifo-1(kc3)IV* and BJ143 *ifo-1(kc3)IV*. Transgenic fluorescent *ifo-1* strains were BJ154 *kcEx28[ifo-1::yfp;myo-3p:mcherry]*, BJ155 *kcEx29[ifo-1::cfp;myo-3p::mcherry]*, BJ156 [*ifb-2::cfp(kcIs21[ifb-2::cfp])V;ifo-1(kc2)IV;kcEx28 [ifo-1::yfp(+);myo-3p::mcherry]* and BJ186 *kcIs30[ifo-1::yfp;myo-3p::mcherry]*.

RNA-mediated interference

RNAi by 'feeding' was performed as described (Hüsken et al., 2008; Kamath et al., 2001). RNAi clones were either obtained from the Ahringer RNAi-library (Geneservice) or corresponding cDNAs (provided by Y. Kohara, National Institute of Genetics, Mishima, Japan) were cloned into the 'feeding' vector. The specificity of each 'feeding' clone was confirmed by sequencing.

Isolation and identification of *ifo-1* mutants

BJ52 worms were treated with 47 mM ethylmethane sulfonate (EMS) for 4 hours at room temperature. F2 progeny was screened for individuals displaying IFB-2::CFP alterations. Isolated worms carrying alleles *kc2* and *kc3* were backcrossed five times with N2 obtaining strains BJ133 and BJ134, respectively. A complementation assay was carried out to show that both mutant strains contain allelic variants of the same gene. To identify the mutated gene, SNP-mapping was performed for the *kc2* allele (Davis et al., 2005). Subsequent RNAi experiments by 'feeding' against the candidate genes within the mapped region were carried out.

Antibody preparation, immunostaining and fluorescence labeling

Antibodies against IFO-1 were prepared in guinea pigs against synthetic peptides (Fig. 2B′) and affinity purified (Peptide Specialty Laboratories). For immunohistology, embryos and larvae were permeabilized using the freeze-crack method (Strome and Wood, 1983) and subsequently fixed as described earlier (van Fürden et al., 2004). Intestine dissections were performed as described previously (McCarter et al., 1997; Strome, 1986). The following primary antibodies were used: guinea pig anti-IFO-1 (1:100), mouse monoclonal anti-actin (Clone: C4; MP Biomedicals; 1:200), guinea pig anti-IFC-2 (1:10) (Karabinos et al., 2002), rabbit anti-DLG-1 (1:200) (Segbert et al., 2004), rabbit anti-ERM-1 (1:200) (van Fürden et al., 2004), mouse monoclonal anti-IFB-2 (MH33; 1:200) and anti-AJM-1 (MH27; 1:200) (Francis and Waterston, 1985). Secondary antibodies (1:200) were Cy2-, Cy3- (Rockland) and AlexaFluor488-conjugated affinity-purified anti-mouse IgG (Invitrogen), Cy2- and Cy3-conjugated affinity-purified anti-guinea pig IgG and Cy2-conjugated anti-rabbit IgG from Jackson ImmunoResearch Laboratories. To quantify actin filaments, AlexaFluor488-phalloidin (Molecular Probes) and anti-actin antibodies were used. Embryos and isolated intestines were permeabilized and fixed as described previously (van Fürden et al., 2004). As a quality control and for identification of intestinal actin localization, dissected intestines were co-stained with antibodies against IFB-2 or DLG-1. To label the intestinal lumen and to check for intestinal tightness, worms were incubated for 30 minutes in PBS containing 5 mg/ml Texas Red-conjugated dextrane (40,000 MW; Molecular Probes) and subsequently rinsed several times in M9 medium.

Microscopy and image processing

Microscopy was performed by confocal laser scanning (LSM 510 META and LSM 710, Zeiss; TCS SP5, Leica) and Nomarski optics using a Zeiss Axioplan 2 fitted with an ORCA-ER (Hamamatsu) camera. Fluorescence signals were quantified after summing the slices in the stack ('sum slices projection') using Fiji software (http://fiji.sc/wiki/index.php/Fiji) and by manually delineating the region of interest. Electron microscopy was carried out as described (Hüsken et al., 2008). Sections were viewed with an EM 10 (Zeiss) and images were recorded with a MegaView III (Olympus) camera.

RESULTS

Alleles *kc2* and *kc3* prevent correct perilumenal network localization of IFB-2

A classical F2 EMS mutagenesis screen was performed to identify genes affecting IF organization in the *C. elegans* intestine. Stable transgenic strain BJ52 *kcIs21[ifb-2::cfp]V* producing IFB-2::CFP was used (Hüsken et al., 2008). The reporter shows a distinct apical localization in the intestine of adult hermaphrodites (Fig. 1A,B). Ten thousand haploid genomes were screened. Alleles *kc2* (strain BJ133) and *kc3* (strain BJ134) exhibited aberrant IFB-2::CFP distribution (Fig. 1C-F). IFB-2::CFP was almost absent from the apical domain in *kc2* mutants. Instead, it accumulated in the cytoplasm in form of granules and presented a continuous junction-like enrichment at the apical cell-cell borders (Fig. 1C,D). During early morphogenesis (1.5-fold stage), IFB-2-labeling surrounded the entire intestinal lumen in the WT (Fig. 1G), whereas only fluorescent spots were seen at the apical domain of intestinal cells of *kc2* mutants (Fig. 1J). Differences persisted during later embryonal and larval stages when a junction-like IFB-2 distribution developed and multiple cytoplasmic granules appeared in the mutant (Fig. 1K,L). By contrast, perilumenal fluorescence was maintained in the WT (Fig. 1H,I). Cytoplasmic granules were also frequently seen in the WT. In comparison to *kc2* mutants, the altered IFB-2::CFP phenotype was less prominent in *kc3* homozygotes becoming manifest only in young adult worms (Fig. 1F) and progressing in older worms.

kc2 and *kc3* are allelic variants of *ifo-1*, which encodes a novel histidine-rich, polyproline tract-containing nematode protein

SNP-mapping was carried out to map the *kc2* and *kc3* alleles (Davis et al., 2005). Both alleles localized to chromosome IV with a similar subchromosomal amplification pattern, indicating that they are variants of the same gene. To examine this possibility, a complementation assay was performed. The F1 non-complementation showed that *kc2* and *kc3* are indeed alleles of the same gene. SNP-based interval mapping was therefore only carried out for *kc3*, narrowing down the genomic localization to within 0.8 Mb harboring 174 protein-coding genes. To identify the affected gene, 124 RNAs were downregulated using bacterial strains of the Ahringer RNAi-library. Only RNAi against the transcript of gene F42C5.10 copied the *kc2*/*kc3* phenotype (Fig. 2A). The gene was named *ifo-1* (intestinal filament organizer) because of the apparent mislocalization of IFB-2 in mutated F42C5.10. It is also referred to as *ttm-4* (Kao et al., 2011). The coding region of the *ifo-1* gene, for which only a single gene model is presented in WormBase, is 5932 bp long and consists of 13 exons (Fig. 2B). A 3879 bp-long mRNA is created after splicing encoding a 1292 amino acid-long protein with a calculated molecular mass of 148.49 kDa and an estimated isoelectric point (IEP) between 5.84 and 6.28 (Fig. 2B′). The *ifo-1* mutations of the *kc2* and *kc3* alleles were identified by sequencing (Fig. 2B). A C→T point mutation was detected in *kc2*
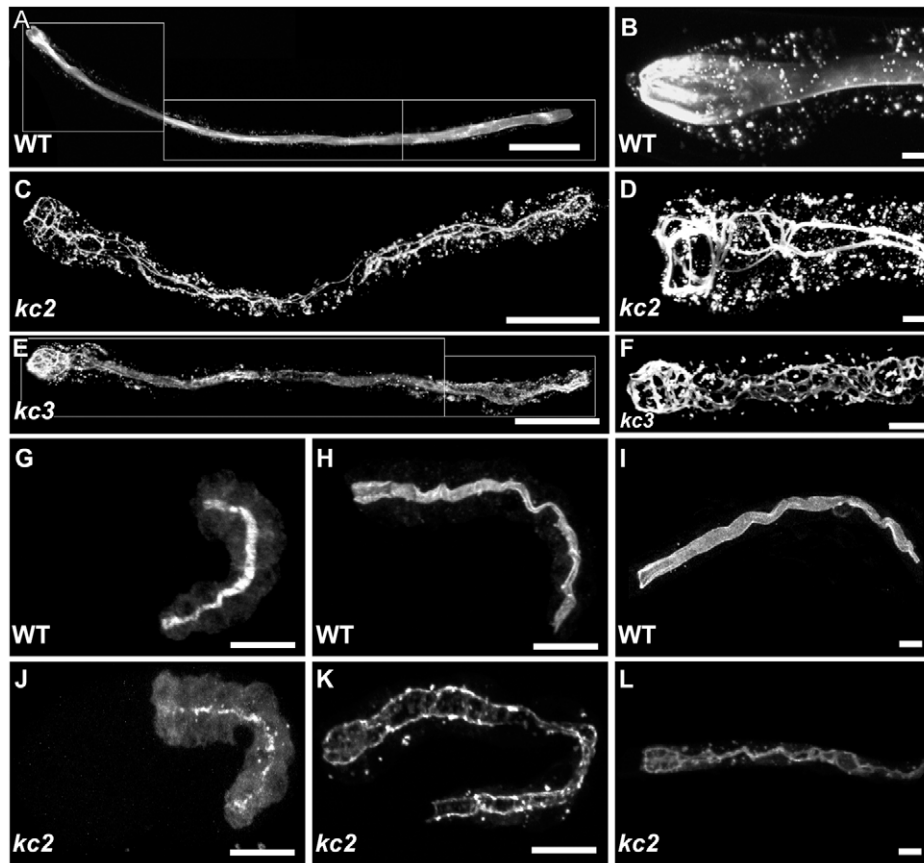
Fig. 1. EMS mutagenesis induces mislocalization of IFB-2::CFP. (A-L) The fluorescence images show the IFB-2::CFP reporter distribution in WT background (strain BJ52; A,B,G-I) and *kc2* (C,D,J-L) and *kc3* (E,F) mutant worms of strains BJ133 and BJ134, respectively. (A-F) Adult worms; (G,H,J,K) embryos; and (I,L) L1 larvae. In WT adults, IFB-2::CFP localizes to the subapical perilumenal cytoskeletal network of intestinal cells (A). By contrast, in *kc2* mutants IFB-2::CFP forms multiple cytoplasmic aggregates and is almost completely absent from the apical part of the cell except for a characteristic rope ladder-type pattern (C). B and D show magnifications of the anterior parts of WT and *kc2* mutant adults, respectively. Young *kc3* adults (<3 days) develop a less severe phenotype than *kc2* with fewer cytoplasmic aggregates and only some small gaps in the subapical IFB-2::CFP network (E). In older adult worms (>3 days), however, the phenotype becomes more severe, as the gaps become bigger and cytoplasmic aggregates increase in size and number (F). In WT embryos, IFB-2 localizes to the apical membrane domain in mid-morphogenesis (G). A diffuse cytoplasmic staining can be observed which becomes weaker during further development (2-fold stage, H) and is almost undetectable in L1 larvae (I). In *kc2* mutants, IFB-2 is never properly localized. During mid-morphogenesis (J) and in a 2.5-fold elongated embryo (K) only a punctate IFB-2 pattern is seen. In the L1 larvae, IFB-2 localizes in a rope ladder pattern at the cell apex and in cytoplasmic aggregates (L). Scale bars: 100 μm in A,C,E; 15 μm in G,H,J,K; 10 μm in B,D,F,I,L.

at nucleotide position 79 of the first exon converting an arginine codon to a stop codon. Allele *kc3* carries a G→A mutation at nucleotide position 919. This corresponds to the first position of the third intron and probably leads to a splicing defect.

BLAST (Basic Local Alignment Search Tool) searches identified *ifo-1* orthologs in other nematodes, notably *C. remanei*, *C. brenneri*, *C. briggsae*, *C. japonica* and *P. Pacificus* with amino acid identities of 95%, 75%, 44%, 82% and 30% respectively. WormBase lists a human ortholog (ENSP00000252825), which is a 699 amino acid sarcoplasmic reticulum, histidine-rich, calcium-binding protein, which shows only very limited similarity to the IFO-1 carboxyterminus (position 788-1292). Functional assays are certainly required to show the relevance of this homology. Subdomain searches did not identify other orthologs, suggesting that *ifo-1* is nematode-specific.

Most apparent is the abundance of histidines in IFO-1 (Fig. 2B′; total number: 106) comprising 8% of all amino acids, which is significantly higher than the average histidine content of other proteins (2%) (Doolittle, 1989). Interestingly, the mammalian keratin

IF-associated protein filaggrin is also particularly rich in histidines (Listwan and Rothnagel, 2004). Also remarkable is the partial sequence similarity to the *Plasmodium falciparum* histidine-rich protein that is involved in rearrangements of the cytoskeletal cell cortex in so-called knobs occurring in infected erythrocytes (Oh et al., 2000; Pei et al., 2005). Another prominent feature of IFO-1 is the abundance of prolines with two poly-proline tracts between amino acids 557 and 599 (Fig. 2B′). In addition, IFO-1 contains multiple phosphorylation sites with 16 listings in the PHOSIDA posttranslational modification data base (www.phosida.com). Finally, the region between amino acids 657 and 706 (Fig. 2B′) is predicted to form coiled-coils (www.ch.embnet.org).

IFO-1 is expressed in the intestine and colocalizes with but is independent of IFB-2

ifo-1::yfp and *ifo-1::cfp* reporter constructs were used for expression studies. These constructs fully reverted the IFB-2 mislocalization to the WT situation (Fig. 2C-C″), demonstrating that IFO-1::YFP and IFO-1::CFP are functional and report the
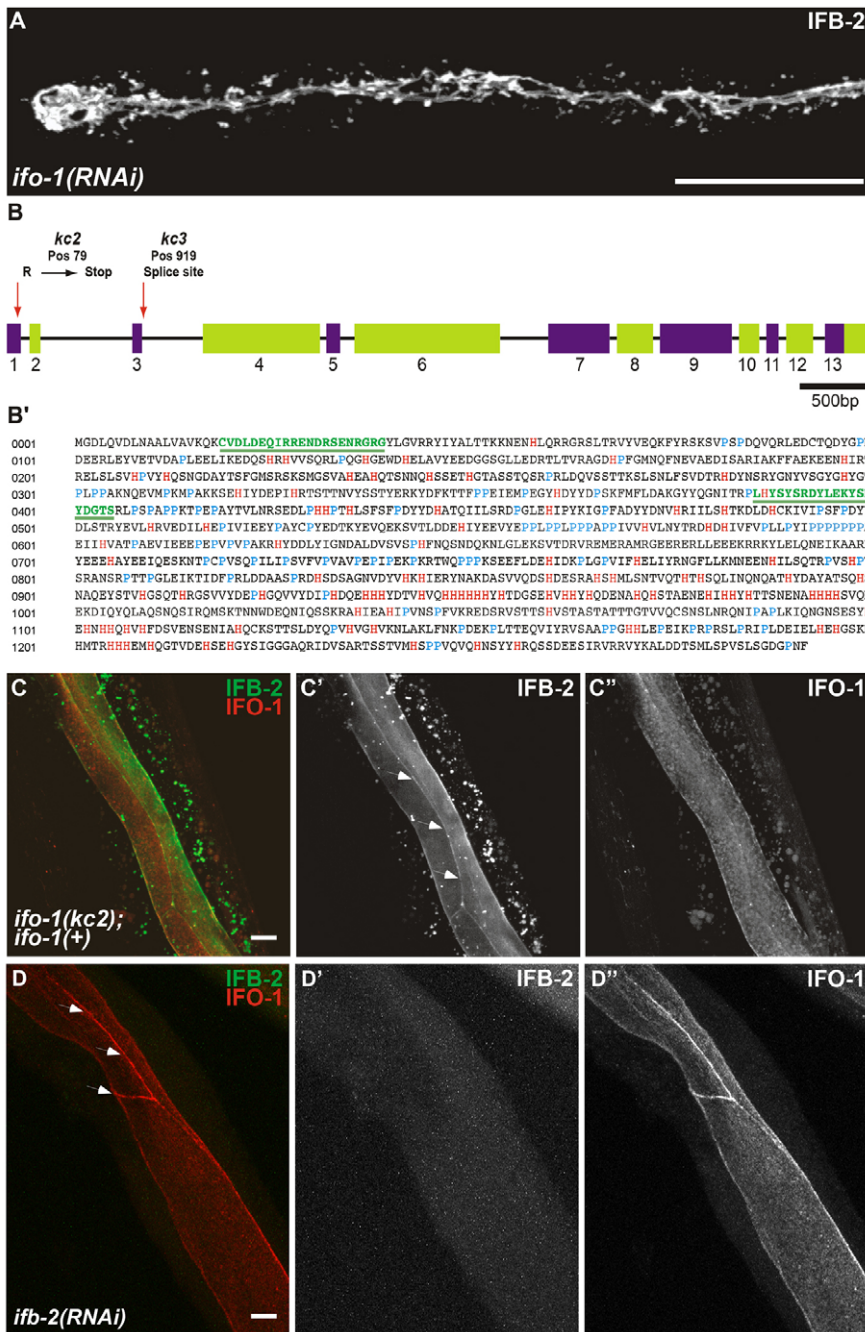
Fig. 2. *kc2* and *kc3* are alleles of gene F42C5.10 encoding intestinal filament organizer IFO-1, which colocalizes with IFB-2. (**A**) Fluorescence image of IFB-2::CFP-expressing reporter strain BJ52 after RNAi against F42C5.10-encoded RNA shows identical phenotype to *kc2* mutant (see Fig. 1C,D). (**B,B′**) Structure of the F42C5.10 *ifo-1* gene and encoded polypeptide sequence. The 5789 bp-long gene consists of 13 exons. Mutant allele *kc2* carries a C→T mutation at position 79 leading to a stop codon in the first exon, *kc3* a G→A mutation at position 919, which is the first position of the 5′ donor splice site of the third intron. The encoded polypeptide, referred to as IFO-1, is 1292 amino acids long. It is rich in histidines (marked in red) and contains a proline-rich region (prolines highlighted in blue). The two peptides (green) used for antibody generation are underlined. (**C-C″**) Fluorescence microscopy of mutant *kc2* worms of strain BJ133 that were microinjected with an *ifo-1::yfp* rescue construct. The normal-appearing, fully rescued IFB-2::CFP fluorescence in green (false color) co-distributes with the IFO-1::YFP fluorescence (false red color). (**D-D″**) Fluorescence microscopy of isolated WT intestines after *ifb-2(RNAi)* that were stained against IFB-2 (false green color) and with purified anti-IFO-1 peptide antibodies (false red color; peptide 2 in B′). Arrows in C′ and D delineate the CeAJ. Scale bars: 50 μm in A; 10 μm in C,D.

distribution of endogenous IFO-1 faithfully. The IFO-1 reporters labeled the perilumenal, subapical cytoplasm of intestinal cells where they co-distributed with IFB-2 (Fig. 2C, Fig. 3A,A′).

To examine the expression of endogenous IFO-1, antibodies were generated against peptides 1 (position 19-39) and 2 (position 386-405; Fig. 2B′). These antibodies stained the intestine in the same fashion as the reporters and anti-IFB-2 antibodies (Fig. 2C-D″, Fig. 3A-D′, Fig. 4A-A″). IFO-1 fluorescence was severely reduced in *kc3* (Fig. 4B-B″) and completely absent in *kc2* (Fig. 4C-C″). These studies also confirmed that IFO-1 is predominantly, if not exclusively, synthesized in the intestine.

Next, the establishment of polarized IFO-1 distribution was examined. At a time at which the diffuse cytoplasmic IFB-2 distribution becomes apically localized, IFO-1 fluorescence was also detectable in the same region, actually slightly preceding

apical IFB-2 deposition (Fig. 3B,B′, arrows). Apical IFO-1 increases in the subsequent 1.5-fold stage were coincident with significant IFO-1 staining of the basolateral cortex (Fig. 3C′). By contrast, IFB-2 was not enriched at the basolateral cortex (Fig. 3C). At the 2- to 3-fold stage, both proteins were almost completely colocalized at the apical membrane domain (Fig. 3D-D′, Fig. 4A-A″). By RNAi we could further show that the apical localization of IFO-1 does not depend on IFB-2 (Fig. 2D-D″).

IFB-2 and IFC-2 are predominantly localized to the CeAJ in *ifo-1* mutants

To find out whether IFO-1 also regulates other IFs, dissected intestines of adult *kc2* worms were stained with antibodies against IFC-2, which has been shown to colocalize with IFB-2 (Hüsken et al., 2008). In *kc2* mutants, IFC-2 showed the same mislocalization
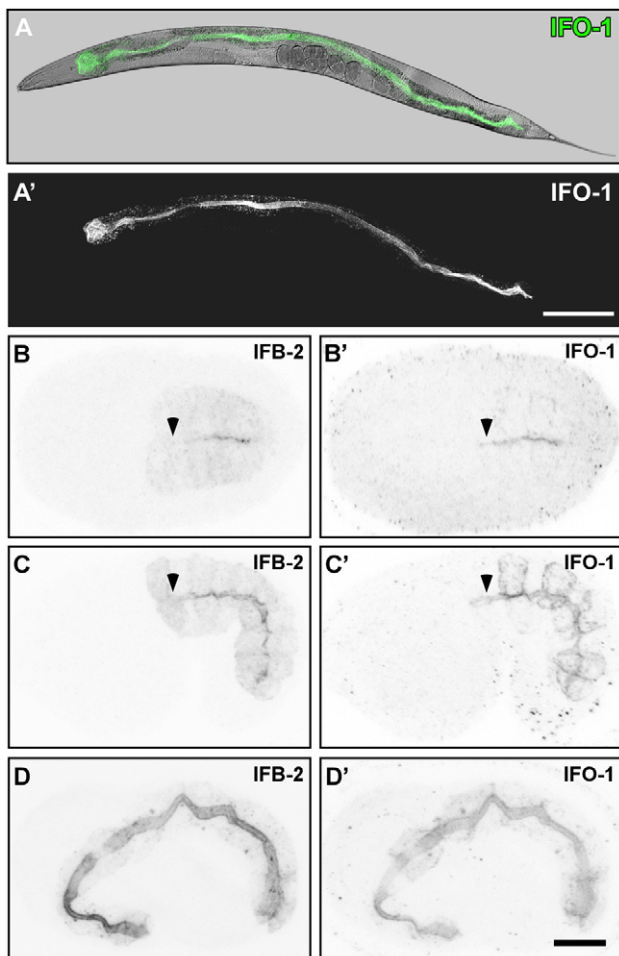
Fig. 3. IFO-1 is expressed exclusively in the intestine and localizes to the adlumenal domain together with IFB-2. Fluorescence and DIC pictures of IFO-1::CFP-expressing adult worm (A,A') and embryos (B-D') of strain BJ155. (**A-A'**) IFO-1 fluorescence (green) is detected in adult worms only in the intestine where it localizes apically (overlay of DIC and fluorescence image in A). (**B-D'**) Embryos co-stained with anti-IFB-2 antibodies show that IFO-1 fluorescence is first detectable during polarization of the intestinal primordium, where it accumulates at the future apical pole together with IFB-2 (B,B'). In mid-morphogenesis, IFO-1 is also present at the lateral cortex that is negative for IFB-2. By contrast, IFB-2 localizes diffusely to the cytoplasm, which is negative for IFO-1 (C,C'). During further development, both proteins continue to accumulate at the apical domain whereas the respective lateral and cytoplasmic fluorescence signals diminish (3-fold embryo in D,D'). Note the absence of anti-IFB-2 signal (arrowheads) in some apical membrane regions that already stain positive for IFO-1::CFP (arrowheads). Scale bars: 100 μm in A'; 10 μm in D' (for B-D').

as IFB-2 with which it co-distributes perfectly (Fig. 5A,A'). To show that overexpression of the IFB-2::CFP reporter is not responsible for the *ifo-1*-phenotype, the mutant alleles *kc2* and *kc3* were outcrossed into the WT background. In the resulting strains, BJ142 (*kc2*) and BJ143 (*kc3*), anti-IFB-2 immunofluorescence showed the same type of mislocalization as in the reporter strains, although the number of cytoplasmic aggregates was slightly reduced (e.g. Fig. 5B).

To demonstrate that IFs accumulate at the CeAJ in *ifo-1* mutants, intestines were co-stained with antibodies against IFB-2 and the CeAJ protein DLG-1 (Fig. 5B,B'). In contrast to the WT (Fig. 6H-

H''), IFB-2 almost completely colocalized with DLG-1 along the entire junctional adhesion belts. The IFB-2 signal, however, protruded slightly from the DLG-1-labeled junction towards the lumen. Dextrane feeding experiments revealed that the junctions were tightly sealed (Fig. 5C,C'). In contrast to the WT, however, lumenal width was highly variable with alternating dilations and constrictions (Fig. 5D,E, arrows), indicative of weakening of the subapical cytoskeleton.

The development of IFB-2 mislocalization was then examined in *kc2* and *kc3* mutant embryos in relation to the CeAJ (Fig. 6). In contrast to the WT situation (Fig. 1G; Fig. 3B,C,D; Fig. 6G-G''), IFB-2 did not accumulate homogenously at the cell apex but was first detected as multiple puncta in proximity to junctional DLG-1 at the 1.5-fold stage of *kc2* mutants (Fig. 6A-A', Fig. 1J). During the following stages, it became increasingly enriched alongside the CeAJ (Fig. 6B-C'). The punctate IFB-2 pattern was substituted by a homogenous junctional localization after hatching at the L1-stage (Fig. 6D,D', Fig. 1L). By contrast, the distribution of IFB-2 was initially indistinguishable from the WT in *kc3* mutants (Fig. 6E,E') and only started to exhibit alterations at the larval stage (Fig. 6F,F'). The perilumenal network became patchy with widening gaps. The full phenotype, similar to that seen in *kc2* mutants, manifested itself only in old adult worms (Fig. 1E,F).

Electron microscopy was performed to search for lumenal and junctional ultrastructural alterations. The WT intestine showed an evenly shaped ellipsoid lumen with regularly arranged brush border-type microvilli (Fig. 7A,D,E). It was surrounded by the electron-dense endotube (Fig. 7A, arrowheads), which is anchored to the CeAJ (Fig. 7A,D,E, arrows). In *kc2* mutants, the lumen was distorted and even branched in some instances (Fig. 7B; data not shown). Most remarkably, the endotube was not detectable (Fig. 7B,C,F). Instead, extensive accumulations were visible at the CeAJ (Fig. 7B,C,F, white arrowheads). This material probably corresponds to the IFB-2/IFC-2-positive junctional structures detected by immunofluorescence.

To examine the consequence of the altered intestine in *ifo-1* mutants for the whole animal, body size was measured. *kc2* mutants were significantly shorter (950 μm; $n=35$; $P<0.0001$) than the WT (1419 μm; $n=35$) and thinner (67 μm versus 87 μm; $n=35$; $P<0.0001$), suggesting a nutritional deficiency. This interpretation was further supported by the observation of significantly reduced progeny (84 ± 36 in *kc2*, $n=51$; $P<0.0001$ versus 238 ± 40 in WT, $n=54$) but no significant embryonic lethality occurred (data not shown). In the mammalian system, depletion of keratins has been shown to reduce glucose uptake by less efficient targeting of glucose transporters to the apical plasma membrane of embryonic epithelia and consequent embryonal growth retardation (Vijayaraj et al., 2009). The absence of a proper IF cytoskeleton in the *C. elegans* intestine might have a similar effect on polarized vesicle trafficking.

LET-413 but not DLG-1, the catenin–cadherin complex (CCC) or CRB-1 is needed for apical localization of IFO-1

To identify regulators of IFO-1 localization, we knocked down known CeAJ proteins and analyzed the distribution of IFO-1. RNAi was performed to reduce the apical CCC components HMR-1/cadherin, HMP-1/α-catenin and HMP-2/β-catenin and the basal DLG-1–AJM-1 complex (DAC) components DLG-1 and AJM-1. In addition, apically localized CRB-1 and basolateral LET-413 were downregulated (Labouesse, 2006; Lynch and Hardin, 2009). In all the experiments, apical IFO-1 was unperturbed (data not
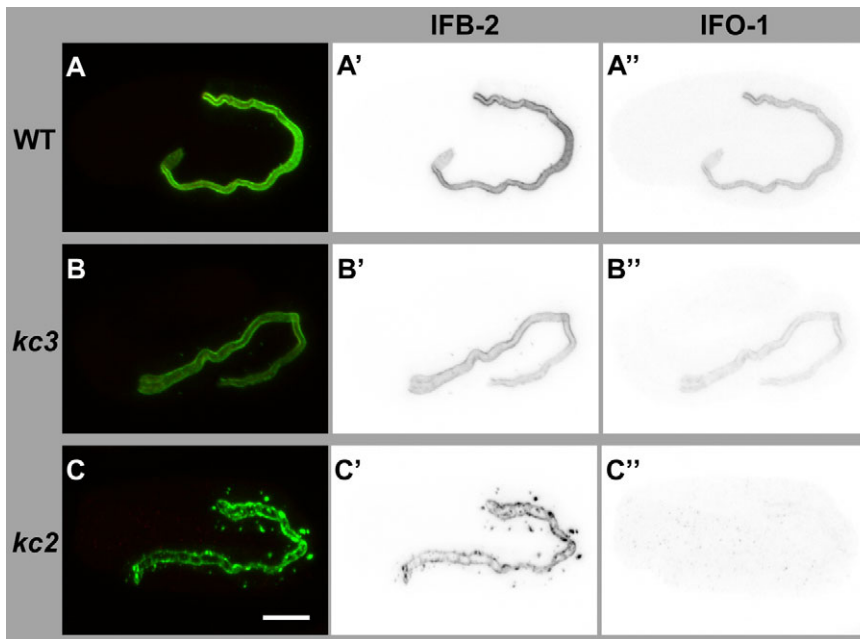
Fig. 4. Peptide antibodies detect IFO-1 exclusively perilumenally in the intestine of WT and at reduced levels of *kc3* mutants but not in the intestine of *kc2* mutants. (A-C″) The images show immunofluorescence analyses (overlay at left; inverse presentation in middle and right column) of WT (A-A″), *kc3* (B-B″) and *kc2* (C-C″) 2-fold embryos that were stained against IFB-2 (green) and with purified anti-IFO-1 peptide antibodies (red; peptide 2, see Fig. 2B′). The micrographs that were taken under the same conditions show a decrease of intestinal IFO-1 in *kc3* (B″) and a complete loss of the protein in *kc2* (C). Scale bar: 10 µm.

shown). The only exception was noted in the *let-413* RNAi experiments that induced an altered distribution of IFO-1::YFP and also of IFB-2 to the basolateral surface of intestinal cells (Fig. 8). This result is not surprising because LET-413 is necessary to maintain the entire terminal web and brush border at the apical surface (Bossinger et al., 2004).

ifo-1 interacts genetically with *erm-1* and *dlg-1*

It has been shown that actin is apically enriched in the *C. elegans* intestine (Bossinger et al., 2004). Given the endotube loss in *kc2* mutants, we therefore analyzed actin distribution in dissected adult intestines by phalloidin staining. In *kc2* mutants, the

phalloidin staining was significantly reduced (Fig. 9A-C). This observation was further corroborated by immunofluorescence microscopy using monoclonal actin antibodies (Fig. 9D-F). The reduction was intestine-specific, as it was not observed in other tissues and was not detected by immunoblotting of total worm lysates (data not shown). A decrease of phalloidin staining (mean intensity/pixel) was also observed in *kc2* mutant embryos (Fig. 9I,I′; 55,957±731, *n*=5; *P*<0.0001 versus 82,186±1785 in WT, *n*=5). In accordance with previous results (Bernadskaya et al., 2011; van Fürden et al., 2004), a significant reduction of intestinal actin was also detectable in *erm-1(tm677)* embryos (Fig. 9H,H′; 47,499±572, *n*=5; *P*<0.0001 versus WT). ERM-1 is
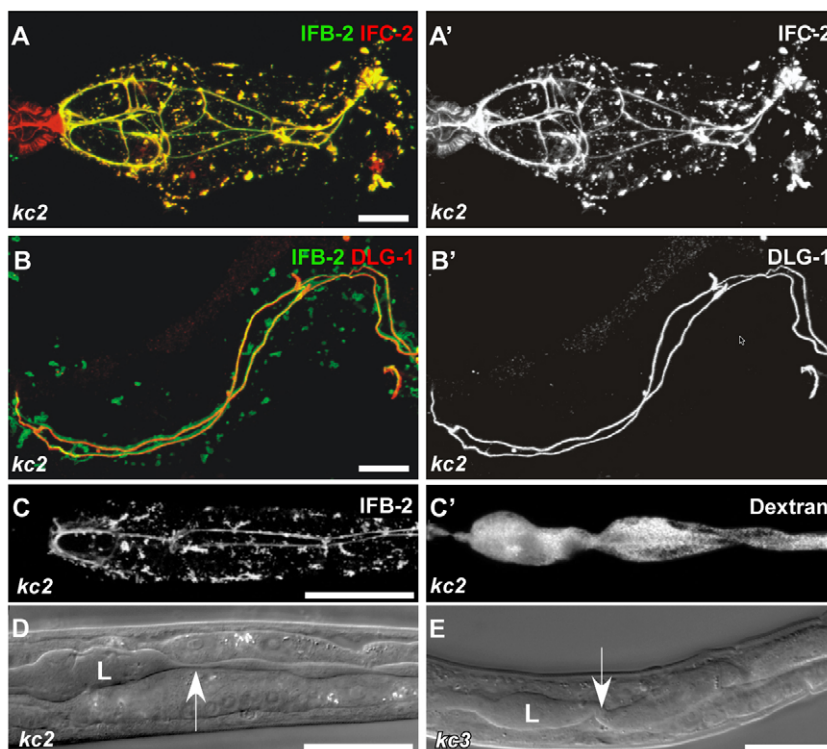

Fig. 5. In *ifo-1* mutant worms, IF proteins IFB-2 and IFC-2 colocalize and co-distribute with the CeAJ marker DLG-1. The intestinal lumen is perturbed but still tight. (A,A′) Fluorescence of dissected adult *ifo-1(kc2)* intestines detecting IFB-2::CFP and anti-IFC-2. IFC-2 colocalizes with IFB-2 in cytoplasmic aggregates and at the CeAJ in anterior intestinal cells. Note the presence of IFC-2 but not of IFB-2 in the adjacent pharynx. **(B,B′)** The re-distributed anti-IFB-2 immunofluorescence colocalizes with anti-DLG-1 immunofluorescence at the CeAJ but shows a more extensive staining adjacent to the junction and in cytoplasmic granules. **(C,C′)** Fluorescence micrographs depict the disturbed IFB-2::CFP distribution in *kc2* mutant worms (strain BJ133) together with TRITC-labeled dextrane that was taken up by feeding. Note that the dextrane is restricted to the altered lumen indicating that the junctional seal is still intact. **(D,E)** DIC micrographs reveal an abnormal lumen (L) with multiple constrictions (arrow) and dilations in *kc2* and *kc3* mutant worms (strains BJ133 and BJ134, respectively). Scale bars: 10 µm in A,B; 100 µm in C-E.

an ezrin-radixin-moesin protein linking actin to the membrane (Fehon et al., 2010; Fiévet et al., 2007). A further decrease in phalloidin staining was noted in *erm-1(tm677);ifo-1(RNAi)* embryos (Fig. 9J,J′; 11,945±45, *n*=5, *P*<0.0001 versus *tm677* and *kc2*). Moreover, an enhanced phenotype was observed for anti-IFB-2 signal (mean intensity/pixel), which was significantly
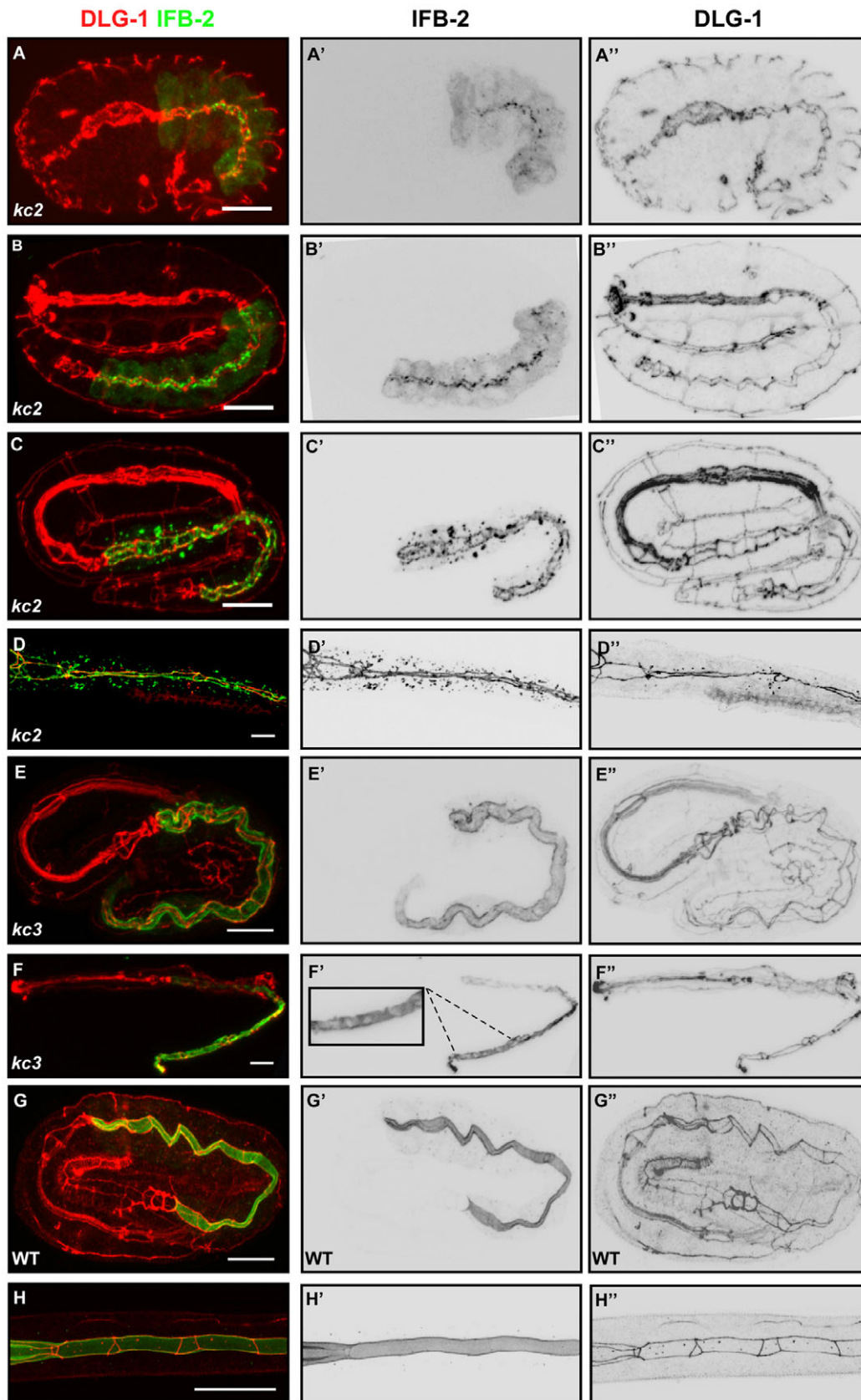

Fig. 6. IFB-2 mislocalization in *kc2* and *kc3* mutants develops differently. Embryos (A-C,E,G) and L1/L2 larvae (D,F,H) were stained with antibodies against IFB-2 (green, A-H; inverted, middle column) and DLG-1 (red, A-H; inverted, right column). (**A-C″**) In the 1.5-fold stage of *kc2* mutants, IFB-2 is localized at the apical part of intestinal cells in a punctate pattern (A-A″), starts to accumulate at the CeAJ at the 2-fold stage but is still present in apical puncta (B-B″) and becomes fully recruited to the CeAJ at the 3-fold stage (C-C″; note increase of cytoplasmic IFB-2 granules in number, especially in the anterior intestine). (**D-D″**) In *kc2* L2, the aggregates further increase and are more evenly distributed throughout the intestine. (**E-E″**) By contrast, IFB-2 is distributed normally in *kc3* embryos (compare with Fig. 3D). (**F-F″**) In the *kc3* L1 stage, small gaps (see magnification in F′) appear in the apical IFB-2-positive network. The gaps increase in size in older worms until the phenotype resembles that of *kc2* worms (see Fig. 1). (**G-H″**) In WT embryos and L1 larvae, the contiguous anti-IFB-2 and anti-DLG-1 signals delineate the endotube and the CeAJ, respectively. Scale bars: 10 μm.
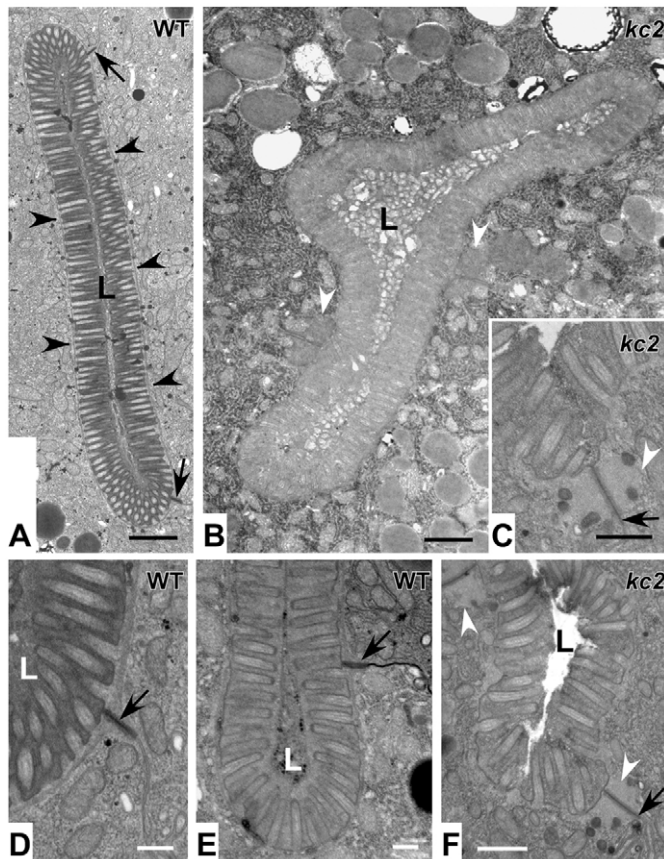
Fig. 7. *ifo-1* mutants lack the prominent endotube and present instead large junctional aggregates. Electron micrographs taken from WT N2 (A,D,E) and strain BJ142 *ifo-1(kc2)* (B,C,F). Note the electron dense endotube in WT (A, black arrowheads), which is absent in *kc2* and the presence of large aggregates (white arrowheads in B,C,F) next to the CeAJ (black arrows). In addition, the lumen (L) is distorted in *kc2* (B) and the microvilli are less ordered (C,F). They still contain, however, characteristic parallel actin filament bundles. Scale bars: 500 nm in A,B; 250 nm in C-F.

Fig. 8: *let-413* RNAi disturbs proper IFO-1 and IFB-2 localization. (**A-B′**) Embryos of reporter strain BJ186 *kcEX28[ifo-1::yfp,myo-3p::mCherry]* were treated with dsRNA directed against either *mtm-6* (A,A′) or *let-413* (B,B′). DIC images (A,B) and corresponding fluorescence micrographs (A′,B′) are shown. Note the typical exclusive apical IFO-1 distribution in the control that contrasts with the circumferential labeling of apical and basolateral cortical domains upon *let-413* RNAi treatment. (**C,C′**) Fluorescence micrographs of 1.75-fold embryo of strain BJ155 *kcEx29[ifo-1::cfp, myo-3p::mcherry]* depicting antibody staining of anti-IFB-2 in C and IFO-1::CFP fluorescence in C′ upon *let-413* RNAi. Note the non-polarized distribution of both. Scale bar: 10 μm.

more reduced in *erm-1(tm677);ifo-1(RNAi)* (31,884±302, *n*=5; *P*<0.0001 versus *tm677* and *kc2*) than in *erm-1(tm677)* (49,283±526, *n*=5) and *kc2* (76,416±1283, *n*=5) (Fig. 9G″-J″; WT: 120,630±2,331, *n*=5). Finally, a novel junctional defect was also detected in *ifo-1(kc2); erm-1(RNAi)* double mutants: in contrast to the respective single mutants, the DLG-1-positive CeAJ and the junctional IFB-2 meshwork was completely disrupted in embryos and L1 larvae, indicative of lumenal discontinuity (Fig. 10A-F″, arrowheads).

To investigate further the genetic interactions of *ifo-1* with the CeAJ, we focused on *dlg-1*, because DLG-1 mutations have been shown to induce junctional defects (e.g. Lockwood et al., 2008) and reduction of apical F-actin (Bernadskaya et al., 2011). In *ifo-1(kc2);dlg-1(RNAi)* embryos, junctional pattern disruption was detectable (Fig. 10G, arrowhead). In addition, junctional IFB-2 was released into the cytoplasm where it formed granular aggregates (Fig. 10H), suggesting that DLG-1 mediates junctional IF anchorage in *kc2*. By contrast, combined reduction of IFO-1 and HMR-1/E-cadherin did not generate junctional disruption and IFB-2 release (Fig. 10I).
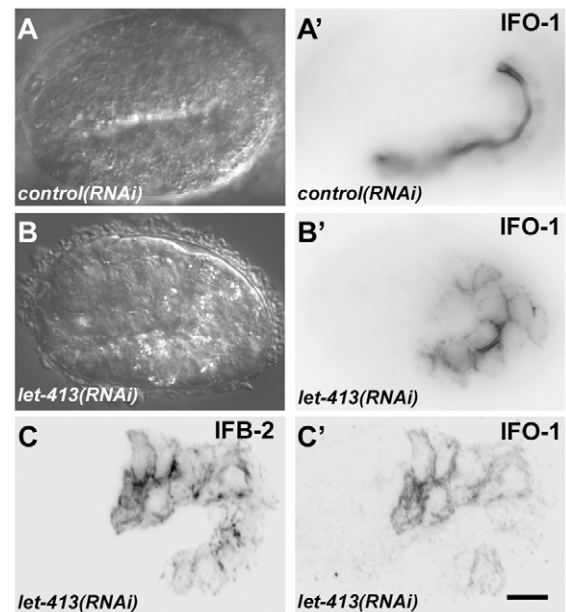
DISCUSSION
IFO-1 is a novel type of cytolinker of the intestinal terminal web

The complexity and structural order of the apical intestinal cytoskeleton is striking. The densely packed and evenly sized microvilli with their core of parallel AFs are anchored to the apical cytoplasm by the terminal web, a complex mesh of filamentous proteins that is anchored to the plasma membrane and connects to the underlying IF cytoskeleton (Brunser and Luft, 1970). Early on, linkers between the different components have attracted attention but their molecular nature is still not fully resolved (Bement and Mooseker, 1996; Hirokawa et al., 1982). With respect to the IF system, the cytolinkers plectin and plastin 1 might fulfill such functions. Both are capable of binding to AFs and IFs and have been localized to the apical cytoplasm in intestinal cells (Grimm-Günter et al., 2009; Nikolic et al., 1996; Steinböck et al., 2000; Wiche et al., 1993). In the case of plastin 1, the functional importance of its linking function was assessed in murine knockouts, in which disruption of the terminal web was observed (Grimm-Günter et al., 2009). In contrast to the *ifo-1* mutants, IF aggregates were not detected in these knockouts. Whether either one or both molecules play such a role in the *C. elegans* intestine is not known. Although the plectin ortholog VAB-10B has been localized to the intestine (Bosher et al., 2003), the expression of the plastin ortholog PLST-1 has not been investigated to date. The identification of
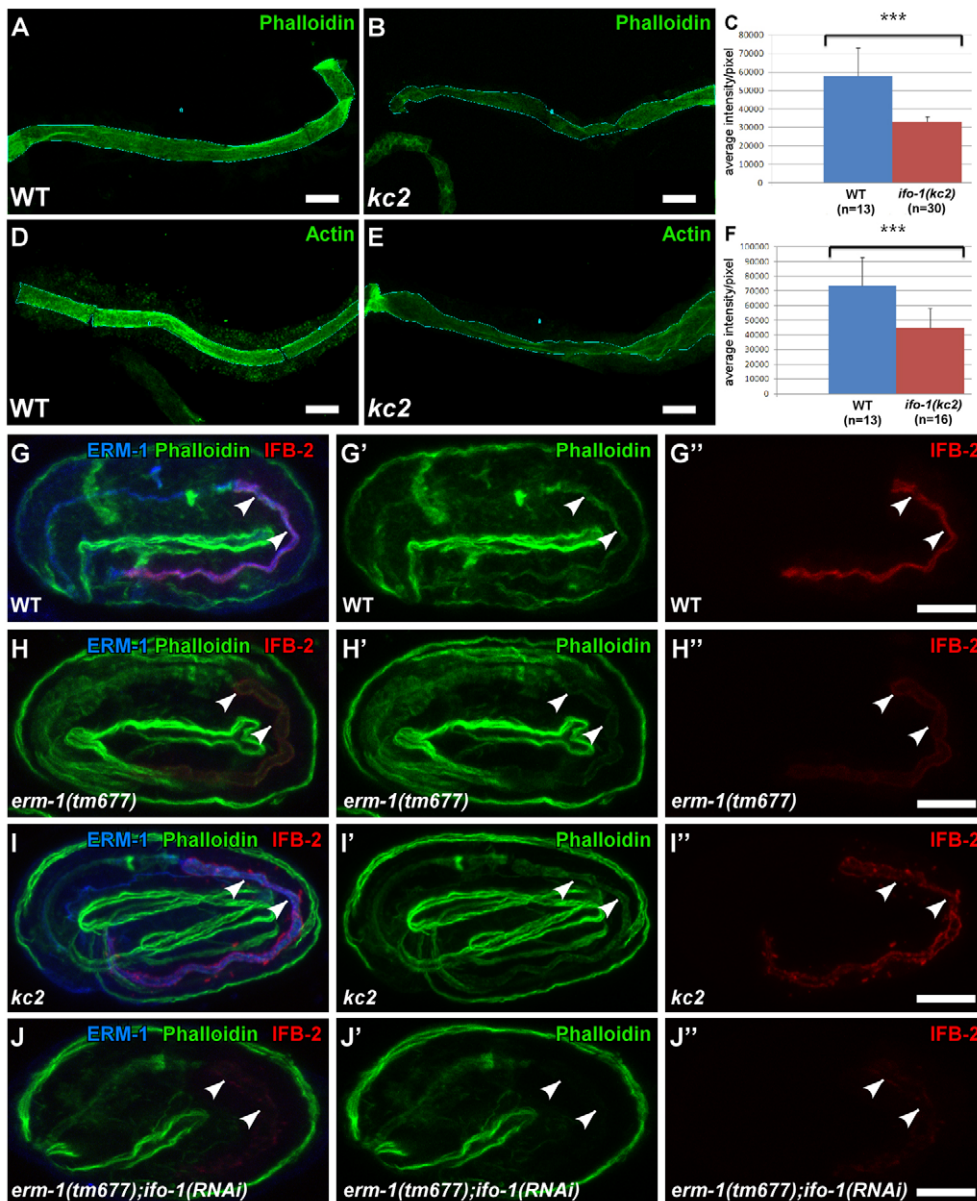
Fig. 9. *ifo-1* mutants show reduced intestinal F-actin and are synthetic with *erm-1*.
(**A-F**) Detection of F-actin either by phalloidin staining (A,B) or by antibodies against F-actin (D,E) of isolated adult intestines (WT in A,D; *ifo-1(kc2)* in B,E) reveals a significant reduction in fluorescence (quantification in C,F; *P*<0.001). Error bars represent s.d. (**G-J″**) Anti-ERM-1 (blue) and anti-IFB-2 (red) immunofluorescence and phalloidin (green). The position of the intestinal lumen is marked by arrowheads. Representative images were taken under the same conditions. Note normal localization of ERM-1 in *kc2* (I) and absence of anti-ERM-1 signal in *tm677* (H,J). (G′-J″) Selective reduction of intestinal phalloidin labeling and anti-IFB-2 immunofluorescence (see Results for quantification) in comparison with WT (G′,G″) is detectable in *erm-1(tm677)* (H′,H″) and in *kc2* (I′,I″) embryos. Note the synthetic phenotype resulting in strong reduction of intestinal phalloidin (J′) and IFB-2 (J″) in *erm-1(tm677);ifo-1(RNAi)* embryos. Scale bars: 10 µm.

IFO-1, however, adds another candidate that affects both the IF and actin systems. It further highlights the importance of coupling both systems for the specific challenges of the nematode intestine.

IFO-1 is needed for establishment and maintenance of the apical IF anchorage in the *C. elegans* intestine

Two *ifo-1* alleles were characterized in this study. Allele *kc2* is most likely to be a null mutation, because only the first 26 codons will be properly translated and both peptide antibodies directed against further downstream epitopes did not detect any epitope in *kc2* mutants. The complete absence of IFO-1 prevented the formation of a circumferential perilumenal IF network, although the apical junction was enriched with IF polypeptides, showing that this localization is independent of IFO-1. RNAi experiments further suggested that junctional localization is dependent on DLG-1. By contrast, IFO-1 is essential for attachment/anchorage of IFs to the submicrovillar region.

By contrast, perilumenal IF network formation occurs normally in *kc3* mutants. This suggests that this mutant is hypomorphic. The identified mutation in the 5′-splice site of intron 3 supports this notion. Apparently, splicing is not completely abrogated, thereby allowing production of a reduced amount of IFO-1. If proper splicing would not occur, a truncated protein of 81 amino acids would be expected containing only the 78 amino-terminal amino acids of IFO-1. The manifestation of a mutant phenotype in later developmental stages, however, further suggests that IFO-1 is crucial for maintenance of the perilumenal IF network. Interestingly, appearance of the phenotype coincides with food uptake and progresses continuously with age. This is reminiscent of the weakening of the endotube in *ifc-2* RNAi-treated worms, which was interpreted as a result of wear and tear induced by the various types of mechanical, chemical and microbial stressors (Hüsken et al., 2008). It might, therefore, be no coincidence that *ifo-1* was recently identified in a screen for cellular responses to pore-forming toxins (Kao et al., 2011). It is attractive to speculate that
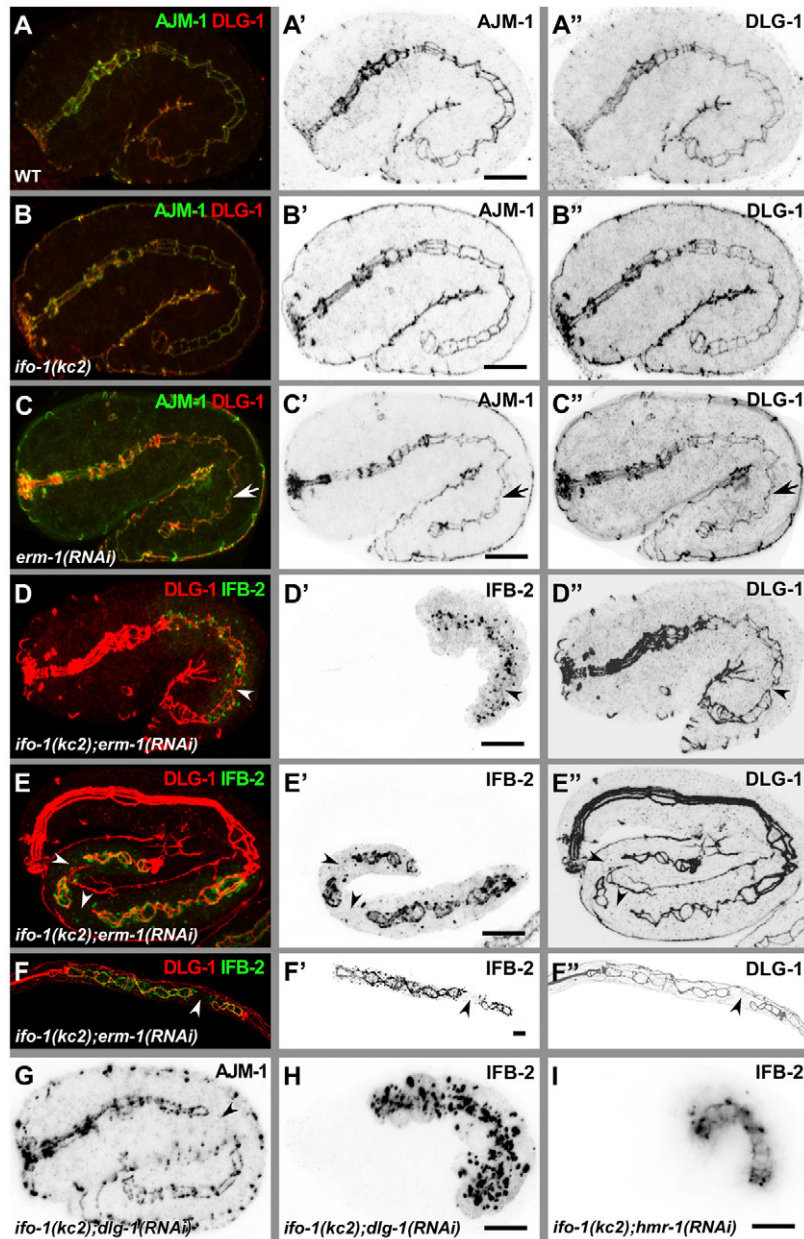
Fig. 10. *ifo-1* **mutants are synthetic with** *erm-1* **and** *dlg-1* **mutants but not with** *hmr-1* **mutants.**
(**A-C″**) Anti-AJM-1 (green in A-C; inverted in A′-C′) and anti-DLG-1 (red in A-C; inverted in A″-C″) immunofluorescence in 1.75-fold stages of WT (A-A″), *ifo-1(kc2)* (B-B″) and after RNAi against *erm-1* (C-C″). Arrow indicates constriction of the future lumen. (**D-F″**) Fluorescence micrographs of IFB-2::CFP (green in D-F; inverted in D′-F′) and anti-DLG-1 signal (red, D-F; inverted D″-F″) in *kc2* background of 1.75-fold embryo (D-D″), 3-fold embryo (E-E″) and L1-larva (F-F″) treated with dsRNA against *erm-1*. (**G,H**) Immunofluorescence of AJM-1 (G) and IFB-2 (H) in 1.75-fold *ifo-1(kc2);dlg-1(RNAi)* embryo. Note that the apical junctional patterns are identical in WT, *ifo-1(kc2)* and *erm-1(RNAi)* but presents disruptions in the double mutants (arrowheads in D-G) as illustrated by discontinuous DLG-1 (D″-F″) and AJM-1 (G) immunofluorescence. Also note the discontinuity in IFB-2 in *ifo-1(kc2); erm-1(RNAi)* (D′-F′) and the complete release of IFB-2 from junctions into cytoplasmic granules in *ifo-1(kc2);dlg-1(RNAi)* (H). (**I**) IFB-2::CFP in vivo fluorescence of an embryo treated with RNAi against *hmr-1* in *kc2* background. Note the continuous fluorescence pattern. Scale bars: 10 μm.

the protective function is mediated by tightening the linkage between the IF cytoskeleton and other components of the supapical cytoplasm in intestinal cells.

IFO-1 acts in concert with ERM-1 and DLG-1 on the organization of the apical intestinal cytoskeleton to preserve epithelial integrity

The apical intestinal cytoplasm contains both filamentous microvillar actin and, basal to this, filamentous terminal web actin that is thought to associate with the CeAJ (Labouesse, 2006). The significant reduction of actin in the absence of IFO-1 is remarkable, as microvillar actin appeared to be still intact as assessed by electron microscopy. This suggests that the loss of actin selectively affects terminal web actin and/or actin of the microvillar rootlets that extend into the apical cytoplasm. This is different from the phenotype observed in animals treated with *erm-1* RNAi. In this instance, a loss of microvilli was described (Göbel et al., 2004), reminiscent of the phenotype observed in worms with mutated *act-*

5, which codes for the specific microvillar actin isoform 5 (MacQueen et al., 2005). Thus, IFO-1 and ERM-1 affect actin organization differently. One possibility is that ERM-1 mediates attachment of actin, specifically of ACT-5, to the apical membrane whereas IFO-1 links ACT-5 and/or other actin isoforms (e.g. those of the terminal web) to the IF network of the endotube. In support of this, a relationship between the presence/absence of an intact IF cytoskeleton and actin was reported for murine colonocytes. Deletion of the IF protein keratin 8 perturbed actin localization, which became depleted in the lateral cortex and patchy in the apical domain (Toivola et al., 2004). A loss of apical F-actin was also noted in cultured colonic cells of line CACO-2 upon downregulation of keratin 8. Of note, this phenotype could be rescued by overexpression of ezrin (Wald et al., 2005).

Conversely, it is not clear at present whether the apical actin cytoskeleton is a prerequisite for correct localization of intestinal IFs. RNAi against components of the WAVE/SCAR complex and *erm-1* weaken the actin cytoskeleton, as revealed by phalloidin
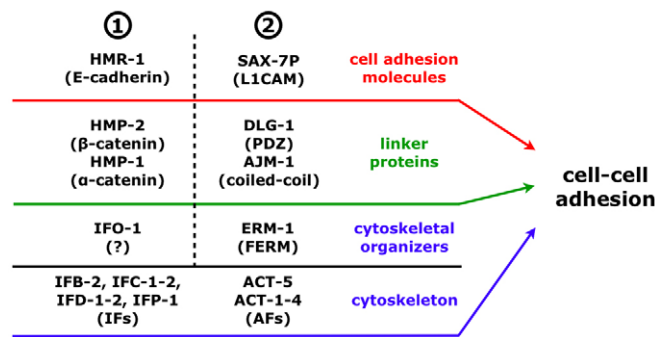
Fig. 11. Model of cell-cell adhesion during organogenesis of the *C. elegans* intestine. Genetic data suggests that in the intestine at least two redundant cell-cell adhesion systems (1 and 2) are involved in apical junction and lumen formation, which both act at the level of cell adhesion molecules, linker proteins and cytoskeletal organizers (note that only the phosphorylated form of SAX-7, SAX-7P, localizes at the CeAJ) (Chen et al., 2001). At the core of each system, linker proteins and cytoskeletal organizers strongly interfere with the localization of cell-cell adhesion molecules and IFs/AFs, respectively, but in both systems these molecules are not predominantly required for each other's localization (e.g. ERM-1 and the DAC still localize apically in *ifo-1(kc2)*; see Fig. 9I, Fig. 10B-B″ and Discussion).

staining, but do not generally interfere with the apical localization of IFB-2 (Bernadskaya et al., 2011; Göbel et al., 2004; Patel et al., 2008; van Fürden et al., 2004) (this study). Although IFO-1 and ERM-1 affect actin organization and distribution of IFs differently, depletion of both proteins enhances reduction of AFs and IFB-2 in the intestine. Taken together, an evolutionarily conserved linkage exists between ERM-type proteins, apical AFs and the IF cytoskeleton in intestinal cells. Species-specific differences exist, however, with respect to the intermediate linkers involved. The particular situation in the mechanically challenged nematode intestine might have necessitated the use of alternative/additional linkers such as IFO-1.

IFO-1 seems to act in concert with ERM-1 and DLG-1 to ensure correct formation of the apical junctional pattern and lumen. The *C. elegans* intestinal tube consists of so-called intestinal rings ('ints'), made up of 1×4 and 8×2 E-cells, which are connected by the CeAJ (Bossinger et al., 2001; Leung et al., 1999; Sulston et al., 1983). Core components of the CeAJ are the CCC (Costa et al., 1998; Kwiatkowski et al., 2010) and the DAC (Bossinger et al., 2001; Firestein and Rongo, 2001; Köppen et al., 2001; Lockwood et al., 2008; McMahon et al., 2001). During morphogenesis of the *C. elegans* intestine, only double knockdowns of HMP-1/α-catenin and DLG-1 (Segbert et al., 2004) or HMR-1/cadherin and ERM-1 but not DLG-1 and ERM-1 (van Fürden et al., 2004) or IFO-1 and HMR-1 (Fig. 10I) generate a similar phenotype as that observed after depletion of IFO-1 and ERM-1 (Fig. 10D-F″) or IFO-1 and DLG-1 (Fig. 10G). These genetic data suggest two parallel pathways, IFO-1/CCC and ERM-1/DAC, that are both necessary to ensure junctional and lumenal integrity presumably by promoting cell-cell adhesion (Fig. 11). HMP-1 contains a functional C-terminal F-actin-binding domain. However, neither full-length HMP-1 nor a ternary complex of HMP-1–HMP-2–HMR-1 binds F-actin in vitro, suggesting that HMP-1 is auto-inhibited (Kwiatkowski et al., 2010). As has been discussed previously (Kwiatkowski et al., 2010). HMP-1 might link the HMP-2–HMR-1 complex to the actin cytoskeleton either upon

homodimerization in vivo (induced by a putative HMP-1-binding protein) or as a monomer upon activation by an additional protein. IFO-1 could be such a protein. In case of the ERM-1/DAC pathway, the L1CAM SAX-7, a single-pass transmembrane cell adhesion receptor belonging to the immunoglobulin superfamily (Chen and Zhou, 2010), has the potential to interact with ERM-1 and DLG-1. The SAX-7 cytoplasmic tail contains three distinct consensus-binding sites, RGQNYPVSQR, SFIGQY and STFV, for cytoskeletal adaptor proteins (FERM: protein 4.1, ezrin, radixin, moesin), for ankyrin and for PDZ proteins (PSD95, DlgA, ZO-1), respectively (Zhou et al., 2008). Although loss of SAX-7 seems not to interfere with the junctional localization of the DAC (Bernadskaya et al., 2011), depletion of the DAC disturbs junctional localization of phosphorylated SAX-7 at the CeAJ in the intestine (our unpublished results). Very recently it has been demonstrated that HMR-1/E-cadherin and SAX-7/L1CAM also function redundantly in blastomere compaction and non-muscle myosin accumulation during *C. elegans* gastrulation (Grana et al., 2010).

Competing interests statement

The authors declare no competing financial interests.

References

Bement, W. M. and Mooseker, M. S. (1996). The cytoskeleton of the intestinal epithelium: Components, assembly, and dynamic rearrangements. In *The Cytoskeleton: A Multi-Volume Treatise*, Vol. 3 (ed. E. H. John and F. P. Ian), pp. 359-404. Greenwich, CT: JAI Press.

Bernadskaya, Y. Y., Patel, F. B., Hsu, H. T. and Soto, M. C. (2011). Arp2/3 promotes junction formation and maintenance in the Caenorhabditis elegans intestine by regulating membrane association of apical proteins. *Mol. Biol. Cell* **22**, 2886-2899.

Bosher, J. M., Hahn, B. S., Legouis, R., Sookhareea, S., Weimer, R. M., Gansmuller, A., Chisholm, A. D., Rose, A. M., Bessereau, J. L. and Labouesse, M. (2003). The *Caenorhabditis elegans* vab-10 spectraplakin isoforms protect the epidermis against internal and external forces. *J. Cell Biol.* **161**, 757-768.

Bossinger, O., Klebes, A., Segbert, C., Theres, C. and Knust, E. (2001). Zonula adherens formation in *Caenorhabditis elegans* requires dlg-1, the homologue of the *Drosophila* gene discs large. *Dev. Biol.* **230**, 29-42.

Bossinger, O., Fukushige, T., Claeys, M., Borgonie, G. and McGhee, J. D. (2004). The apical disposition of the *Caenorhabditis elegans* intestinal terminal web is maintained by LET-413. *Dev Biol.* **268**, 448-456.

Brenner, S. (1974). The genetics of *Caenorhabditis elegans*. *Genetics* **77**, 71-94.

Brunser, O. and Luft, H. J. (1970). Fine structure of the apex of absorptive cell from rat small intestine. *J. Ultrastruct. Res.* **31**, 291-311.

Carberry, K., Wiesenfahrt, T., Windoffer, R., Bossinger, O. and Leube, R. E. (2009). Intermediate filaments in *Caenorhabditis elegans*. *Cell Motil. Cytoskeleton* **66**, 852-864.

Chen, L. and Zhou, S. (2010). "CRASH"ing with the worm: insights into L1CAM functions and mechanisms. *Dev. Dyn.* **239**, 1490-1501.

Chen, L., Ong, B. and Bennett, V. (2001). LAD-1, the *Caenorhabditis elegans* L1CAM homologue, participates in embryonic and gonadal morphogenesis and is a substrate for fibroblast growth factor receptor pathway-dependent phosphotyrosine-based signaling. *J. Cell Biol.* **154**, 841-855.

Costa, M., Raich, W., Agbunag, C., Leung, B., Hardin, J. and Priess, J. (1998). A putative catenin-cadherin system mediates morphogenesis of the *Caenorhabditis elegans* embryo. *J. Cell Biol.* **141**, 297-308.

Davis, M. W., Hammarlund, M., Harrach, T., Hullett, P., Olsen, S. and Jorgensen, E. M. (2005). Rapid single nucleotide polymorphism mapping in *C. elegans*. *BMC Genomics* **6**, 118.

Doolittle, R. F. (1989). *Redundancies in protein sequences.* NY: Plenum Press.

Fehon, R. G., McClatchey, A. I. and Bretscher, A. (2010). Organizing the cell cortex: the role of ERM proteins. *Nat. Rev. Mol. Cell Biol.* **11**, 276-287.

Fiévet, B., Louvard, D. and Arpin, M. (2007). ERM proteins in epithelial cell organization and functions. *Biochim. Biophys Acta* **1773**, 653-660.

Firestein, B. L. and Rongo, C. (2001). DLG-1 is a MAGUK similar to SAP97 and is required for adherens junction formation. *Mol. Biol. Cell* **12**, 3465-3475.

Fletcher, D. A. and Mullins, R. D. (2010). Cell mechanics and the cytoskeleton. *Nature* **463**, 485-492.

Francis, G. and Waterston, R. (1985). Muscle organization in *Caenorhabditis elegans*: localization of proteins implicated in thin filament attachment and I-band organization. *J. Cell Biol.* **101**, 1532-1549.

Göbel, V., Barrett, P. L., Hall, D. H. and Fleming, J. T. (2004). Lumen morphogenesis in *C. elegans* requires the membrane-cytoskeleton linker erm-1. *Dev. Cell* **6**, 865-873.

Grana, T. M., Cox, E. A., Lynch, A. M. and Hardin, J. (2010). SAX-7/L1CAM and HMR-1/cadherin function redundantly in blastomere compaction and non-muscle myosin accumulation during *Caenorhabditis elegans* gastrulation. *Dev. Biol.* **344**, 731-744.

Grimm-Günter, E. M., Revenu, C., Ramos, S., Hurbain, I., Smyth, N., Ferrary, E., Louvard, D., Robine, S. and Rivero, F. (2009). Plastin 1 binds to keratin and is required for terminal web assembly in the intestinal epithelium. *Mol. Biol. Cell* **20**, 2549-2562.

Hirokawa, N., Tilney, L. G., Fujiwara, K. and Heuser, J. E. (1982). Organization of actin, myosin, and intermediate filaments in the brush border of intestinal epithelial cells. *J. Cell Biol.* **94**, 425-443.

Hüsken, K., Wiesenfahrt, T., Abraham, C., Windoffer, R., Bossinger, O. and Leube, R. (2008). Maintenance of the intestinal tube in *Caenorhabditis elegans*: the role of the intermediate filament protein IFC-2. *Differentiation* **76**, 881-896.

Hutter, H. (2003). Extracellular cues and pioneers act together to guide axons in the ventral cord of *C. elegans*. *Development* **130**, 5307-5318.

Iwatsuki, H. and Suda, M. (2010). Seven kinds of intermediate filament networks in the cytoplasm of polarized cells: structure and function. *Acta Histochem. Cytochem.* **43**, 19-31.

Kamath, R. S., Martinez-Campos, M., Zipperlen, P., Fraser, A. G. and Ahringer, J. (2001). Effectiveness of specific RNA-mediated interference through ingested double-stranded RNA in *Caenorhabditis elegans*. *Genome Biol.* **2**, research 0002.

Kao, C. Y., Los, F. C., Huffman, D. L., Wachi, S., Kloft, N., Husmann, M., Karabrahimi, V., Schwartz, J. L., Bellier, A., Ha, C. et al. (2011). Global functional analyses of cellular responses to pore-forming toxins. *PLoS Pathog.* **7**, e1001314.

Karabinos, A., Schulze, E., Klisch, T., Wang, J. and Weber, K. (2002). Expression profiles of the essential intermediate filament (IF) protein A2 and the IF protein C2 in the nematode *Caenorhabditis elegans*. *Mech. Dev.* **117**, 311-314.

Karabinos, A., Schunemann, J. and Weber, K. (2004). Most genes encoding cytoplasmic intermediate filament (IF) proteins of the nematode *Caenorhabditis elegans* are required in late embryogenesis. *Eur. J. Cell Biol.* **83**, 457-468.

Kim, S. and Coulombe, P. A. (2007). Intermediate filament scaffolds fulfill mechanical, organizational, and signaling functions in the cytoplasm. *Genes Dev.* **21**, 1581-1597.

Köppen, M., Simske, J. S., Sims, P. A., Firestein, B. L., Hall, D. H., Radice, A. D., Rongo, C. and Hardin, J. D. (2001). Cooperative regulation of AJM-1 controls junctional integrity in *Caenorhabditis elegans* epithelia. *Nat. Cell Biol.* **3**, 983-991.

Kormish, J. D., Gaudet, J. and McGhee, J. D. (2010). Development of the *C. elegans* digestive tract. *Curr. Opin. Genet. Dev.* **20**, 346-354.

Kwiatkowski, A. V., Maiden, S. L., Pokutta, S., Choi, H. J., Benjamin, J. M., Lynch, A. M., Nelson, W. J., Weis, W. I. and Hardin, J. (2010). In vitro and in vivo reconstitution of the cadherin-catenin-actin complex from *Caenorhabditis elegans*. *Proc. Natl. Acad. Sci. USA* **107**, 14591-14596.

Labouesse, M. (2006). Epithelial junctions and attachments (January 13, 2006). In *WormBook* (ed. The *C. elegans* Research Community). doi.org/doi:10.1895/wormbook.1.56.1, http://www.wormbook.org.

Leung, B., Hermann, G. J. and Priess, J. R. (1999). Organogenesis of the *Caenorhabditis elegans* intestine. *Dev. Biol.* **216**, 114-134.

Listwan, P. and Rothnagel, J. A. (2004). Keratin bundling proteins. *Methods Cell Biol.* **78**, 817-827.

Lockwood, C. A., Lynch, A. M. and Hardin, J. (2008). Dynamic analysis identifies novel roles for DLG-1 subdomains in AJM-1 recruitment and LET-413-dependent apical focusing. *J. Cell Sci.* **121**, 1477-1487.

Lynch, A. M. and Hardin, J. (2009). The assembly and maintenance of epithelial junctions in *C. elegans*. *Front. Biosci.* **14**, 1414-1432.

MacQueen, A. J., Baggett, J. J., Perumov, N., Bauer, R. A., Januszewski, T., Schriefer, L. and Waddle, J. A. (2005). ACT-5 is an essential *Caenorhabditis elegans* actin required for intestinal microvilli formation. *Mol. Biol. Cell* **16**, 3247-3259.

McCarter, J., Bartlett, B., Dang, T. and Schedl, T. (1997). Soma-germ cell interactions in *Caenorhabditis elegans*: multiple events of hermaphrodite germline development require the somatic sheath and spermathecal lineages. *Dev. Biol.* **181**, 121-143.

McGhee, J. D. (2007). The *C. elegans* intestine (March 27, 2007). In *WormBook*, (ed. The *C. elegans* Research Community). doi.org/doi:10.1895/wormbook.1.133.1, http://www.wormbook.org.

McMahon, L., Legouis, R., Vonesch, J. L. and Labouesse, M. (2001). Assembly of *C. elegans* apical junctions involves positioning and compaction by LET-413 and protein aggregation by the MAGUK protein DLG-1. *J. Cell Sci.* **114**, 2265-2277.

Munn, E. A. and Greenwood, C. A. (1984). The occurrence of submicrovillar endotube (Modified Terminal Web) and associated cytoskeletal structures in the intestinal epithelia of nematodes. *Philos. Trans. R. Soc. Lond. B Biol. Sci.* **306**, 1-18.

Nikolic, B., Mac Nulty, E., Mir, B. and Wiche, G. (1996). Basic amino acid residue cluster as part of nuclear targeting sequence motif is essential for cytoplasmic plectin-vimentin network junctions. *J. Cell Biol.* **134**, 1455-1467.

Oh, S. S., Voigt, S., Fisher, D., Yi, S. J., LeRoy, P. J., Derick, L. H., Liu, S. and Chishti, A. H. (2000). Plasmodium falciparum erythrocyte membrane protein 1 is anchored to the actin-spectrin junction and knob-associated histidine-rich protein in the erythrocyte skeleton. *Mol. Biochem. Parasitol.* **108**, 237-247.

Patel, F. B., Bernadskaya, Y. Y., Chen, E., Jobanputra, A., Pooladi, Z., Freeman, K. L., Gally, C., Mohler, W. A. and Soto, M. C. (2008). The WAVE/SCAR complex promotes polarized cell movements and actin enrichment in epithelia during *C. elegans* embryogenesis. *Dev. Biol.* **324**, 297-309.

Pei, X., An, X., Guo, X., Tarnawski, M., Coppel, R. and Mohandas, N. (2005). Structural and functional studies of interaction between Plasmodium falciparum knob-associated histidine-rich protein (KAHRP) and erythrocyte spectrin. *J. Biol. Chem.* **280**, 31166-31171.

Segbert, C., Johnson, K., Theres, C., van Fürden, D. and Bossinger, O. (2004). Molecular and functional analysis of apical junction formation in the gut epithelium of *Caenorhabditis elegans*. *Dev. Biol.* **266**, 17-26.

Steinböck, F. A., Nikolic, B., Coulombe, P. A., Fuchs, E., Traub, P. and Wiche, G. (2000). Dose-dependent linkage, assembly inhibition and disassembly of vimentin and cytokeratin 5/14 filaments through plectin's intermediate filament-binding domain. *J. Cell Sci.* **113**, 483-491.

Strome, S. (1986). Fluorescence visualization of the distribution of microfilaments in gonads and early embryos of the nematode *Caenorhabditis elegans*. *J. Cell Biol.* **103**, 2241-2252.

Strome, S. and Wood, W. B. (1983). Generation of asymmetry and segregation of germ-line granules in early *C. elegans* embryos. *Cell* **35**, 15-25.

Sulston, J., Schierenberg, E., White, J. and Thomson, J. (1983). The embryonic cell lineage of the nematode *Caenorhabditis elegans*. *Dev. Biol.* **100**, 64-119.

Toivola, D. M., Krishnan, S., Binder, H. J., Singh, S. K. and Omary, M. B. (2004). Keratins modulate colonocyte electrolyte transport via protein mistargeting. *J. Cell Biol.* **164**, 911-921.

Toivola, D. M., Strnad, P., Habtezion, A. and Omary, M. B. (2010). Intermediate filaments take the heat as stress proteins. *Trends Cell Biol.* **20**, 79-91.

van Fürden, D., Johnson, K., Segbert, C. and Bossinger, O. (2004). The C. elegans ezrin-radixin-moesin protein ERM-1 is necessary for apical junction remodelling and tubulogenesis in the intestine. *Dev. Biol.* **272**, 262-276.

Vijayaraj, P., Kroger, C., Reuter, U., Windoffer, R., Leube, R. E. and Magin, T. M. (2009). Keratins regulate protein biosynthesis through localization of GLUT1 and -3 upstream of AMP kinase and Raptor. *J. Cell Biol.* **187**, 175-184.

Wald, F. A., Oriolo, A. S., Casanova, M. L. and Salas, P. J. (2005). Intermediate filaments interact with dormant ezrin in intestinal epithelial cells. *Mol. Biol. Cell* **16**, 4096-4107.

Wiche, G., Gromov, D., Donovan, A., Castanon, M. J. and Fuchs, E. (1993). Expression of plectin mutant cDNA in cultured cells indicates a role of COOH-terminal domain in intermediate filament association. *J. Cell Biol.* **121**, 607-619.

Zhou, S., Opperman, K., Wang, X. and Chen, L. (2008). unc-44 Ankyrin and stn-2 gamma-syntrophin regulate sax-7 L1CAM function in maintaining neuronal positioning in *Caenorhabditis elegans*. *Genetics* **180**, 1429-1443.